Characteristic Thermal Parameters in Electric Motors: Comparison Between Induction- and Permanent Magnet Excited Machine

Benedikt Groschup, Martin Nell, Florian Pauli, and Kay Hameyer, *Senior Member, IEEE*

***Abstract*—The thermal modeling and design process of highly utilized electric machines is a complex task. The main heat paths within an electric drive are influenced by a variety of different thermal interfaces, that can mainly be described by thermal conduction and convection. The proper selection and estimation of these design parameters is challenging especially in the early design stage. This paper provides a systematic investigation evaluating inaccuracies and design influences of single thermal resistances, such as the convective heat transfer in the rotor-stator annulus, in the cooling jacket or interfaces between different machine components. Within the study, electromagnetic finite element models and thermal lumped parameter models of two traction drives are developed and validated using test bench measurements. The thermal design parameters are varied in a range resulting from intensive literature research and own laboratory experience. The influence of the design parameters in different operational points of the drives are studied in a sensitivity analysis.**

***Index Terms*—Induction machines, permanent magnet machines, thermal parameters, thermal variables measurement, sensitivity analysis, cooling.**

I. Introduction

ADVANCED rotor or stator cooling technologies are used to increase the operational range and power density of electric traction drives [1]. The different cooling locations in the stator or rotor lead to a different potential of increasing the power density [2], [3]. After selecting the cooling technology, a more detailed analysis of the resistances in the heat transition path needs to be performed. Some studies directly focus on specific resistances trying to improve the accuracy of their thermal model. Exemplary studies for the winding system or typical convective heat transfer problems can be found in [4] and [5] respectively. Anyways, a highly accurate description of a single problem has little impact on the overall accuracy of the model in case the studied thermal resistance is not critical to the overall design. In other words, it is crucial to first identify critical parameters of the thermal design before improving single ones. Quantitative values and discussion of critical parameters of industrial motors are given in [5]–[7]. Sensitivity studies of thermal parameters can be found in different investigations in literature such as [8]–[10]. A commonly used approach is the selection of a mean value by literature research, experience or test bench evaluation. The boundaries can then be calculated on a percentage basis such as $\pm 50\%$ [10] or a probability distribution [9]. In this case, the results can be used to estimate the sensitivity of each factor on a percentage basis, but not based on boundaries that are discussed within the community. The studies either focus on particular parameters such as the specific heat transfer from the winding to the housing [10], or study one machine design in one operational point [9], [10]. A comparison for several operational conditions or different machines with varying cooling typologies is not performed.

In this study, a systematic analysis of the thermal design parameters of two different electric traction drives is performed, i.e. a Permanent Magnet Synchronous Motor (PMSM) and an Induction Motor (IM). A fully factorial sensitivity study is used. Eight different thermal parameters are investigated. Each parameter is discussed and upper and lower boundaries for the sensitivity study are selected based on a comprehensive stand of the art analysis. Electromagnetic finite element simulations of each drive are performed to evaluate the losses in the torque-speed map. Thermal network models are developed for each machine. The models are parameterized and calibrated by using test bench measurements. The models are used to study the influence of the eight different thermal parameters on the temperature of the crucial components, i.e. the windings, the magnets and the rotor bar. For each drive, two different operational points are considered, i.e. one operational point in the base speed area and one operational point in the field weakening area.

II. Simulation Model

A. Studied Electric Machine and Electromagnetic Simulation Model

The data sheet of the two studied machines is depicted in Table I. A cross sectional view is shown in Fig. 1. The studied PMSM is equipped with two layers of burried magnets in the rotor. The motor has a peak power S2 of 125 kW. A helix shaped water jacket in the housing is used for heat extraction. The utilized loss calculation methodology in the finite element

Manuscript received July 9, 2020; revised November 4, 2020, November 12, 2020, and January 26, 2021; accepted January 29, 2021. Date of publication February 3, 2021; date of current version August 20, 2021. Paper no. TEC-00706-2020. *(Corresponding author: Benedikt Groschup.)*

The authors are with the Institute of Electrical Machines (IEM), RWTH Aachen University, 52062 Aachen, Germany (e-mail: benedikt.groschup@iem.rwth-aachen.de; martin.nell@iem.rwth-aachen.de; florian.pauli@rwth-aachen.de; kay.hameyer@iem.rwth-aachen.de).

Color versions of one or more figures in this article are available at https://doi.org/10.1109/TEC.2021.3056771.

Digital Object Identifier 10.1109/TEC.2021.3056771

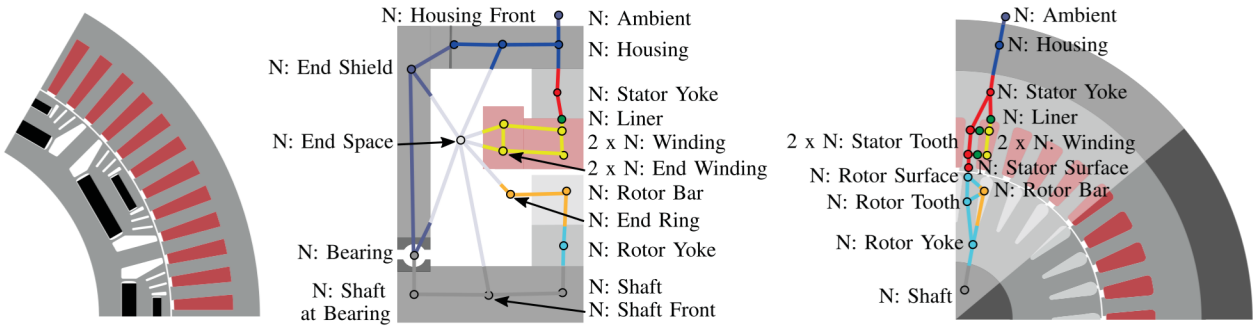

Fig. 1. Cross sectional view of studied PMSM (left) and the studied IM (right) with its thermal nodes.

TABLE I
OVERVIEW OF STUDIED ELECTRIC MACHINES

Specification	Unit	PMSM	IM
number of pole pairs		6	4
stator inner diameter	mm	180	103
active axial length	mm	131	200
rated speed	rpm	4500	3000
rated torque (S1)	N m	210	64
peak power (S2)	kW	125	30

simulation is described in [11]. The studied IM delivers a S2 power of 30 kW. The losses of the IM are calculated using a hybrid simulation approach by coupling static FEA with transient FEA and analytic formulations [12]. The IM is equipped with a forced air cooling in the housing. Fig. 1 includes a description of the location of the thermal nodes in the Lumped Parameter Thermal Network (LPTN). In the middle part of the figure, the axial view of the IM is depicted. The end space is modeled with one node that is connected to the adjacent nodes, i.e. nodes from the winding head, the housing, the end shield, the bearing, and the rotor components. In the axial view, the rotor bar and the end winding are depicted, not the rotor and stator teeth. Thus no connection between the rotor and the stator is visible. This connection can be seen in the right part of the figure. The stator-rotor-surface nodes couple the stator and the rotor over the air gap.

B. LPTN Model

The development of the LPTN for both machines is based on the methodology introduced in [6], [7]. For the PMSM, the LPTN is already introduced in [3]. Some detailed information about the calculation of the thermal resistances for the convective problems in the machine are found in this reference. The LPTN model for the IM is newly developed for this study and depicted in Fig. 2. The description of the nodes is similar to the overview given in Fig. 1. The electromagnetic active part of the IMis modeled with one slice, i.e. the entire lamination stack of rotor and stator is not axially subdivided. The PMSM model is axially subdivided into three parts, because the thermal conductivity of the magnets in axial direction is significantly lower than the axial thermal conductivity of the rotor bar of the IM. The winding is represented by cuboidal elements as introduced in [13]. The three sections of the front-end, middle-part and rear-end of the winding are represented by two cuboidal elements per section. The similar approach is used for the representation of the rotor bar.

III. PARAMETERS OF THE THERMAL MODEL

A. Heat Transfer of the Primary Cooling

The identification of the heat transfer coefficient between the housing and the fluid in the water jacket of the PMSM is based on an analytical approach. The calculated value is parameterized using test bench measurements, as described in [3]. The result of the process is a heat transfer coefficient h of 1400 $\mathrm{W/(m^2\,K)}$. The heat transfer coefficient between the housing and the forced air flow around the housing for the IM is identified to be 80 $\mathrm{W/(m^2\,K)}$. An exact identification of the heat transfer coefficient with analytical formula is not possible, as entrance effects, bending effects, or different hydraulic diameter are not considered in the calculation. For the sensitivity study, the two above mentioned values for the IM and the PMSM are multiplied by a variation factor for the primary cooling k_{pc} of 0.8 and 1.2 of the lower and upper boundary respectively. The location of the according thermal resistance from the housing to the ambient $R_{\mathrm{ho-am}}$ is depicted in Fig. 2.

B. Heat Transfer in Stator Rotor Annulus

The heat transfer problem in the stator rotor annulus in LPTN models is usually modeled using Nusselt-correlations (Nu) defined by two dimensionless numbers. The Taylor-Number (Ta) represents the influence of the rotating inner cylinder. The axial Reynolds-Number (Re_{ax}) represents an axial fluid flow in the annulus. No axial fluid flow is found in both machines, leading to a zero value for Re_{ax}. Different definitions of the Ta-Number can be found in literature. In this study, the definition given by Kaye and Elagar Ta_{KE} is used [14]

$$Ta = Ta_{\mathrm{KE}} = \frac{\omega r_{\mathrm{a}}^{0.5} \delta^{1.5}}{\nu} \cdot F_{\mathrm{G}}, \tag{1}$$

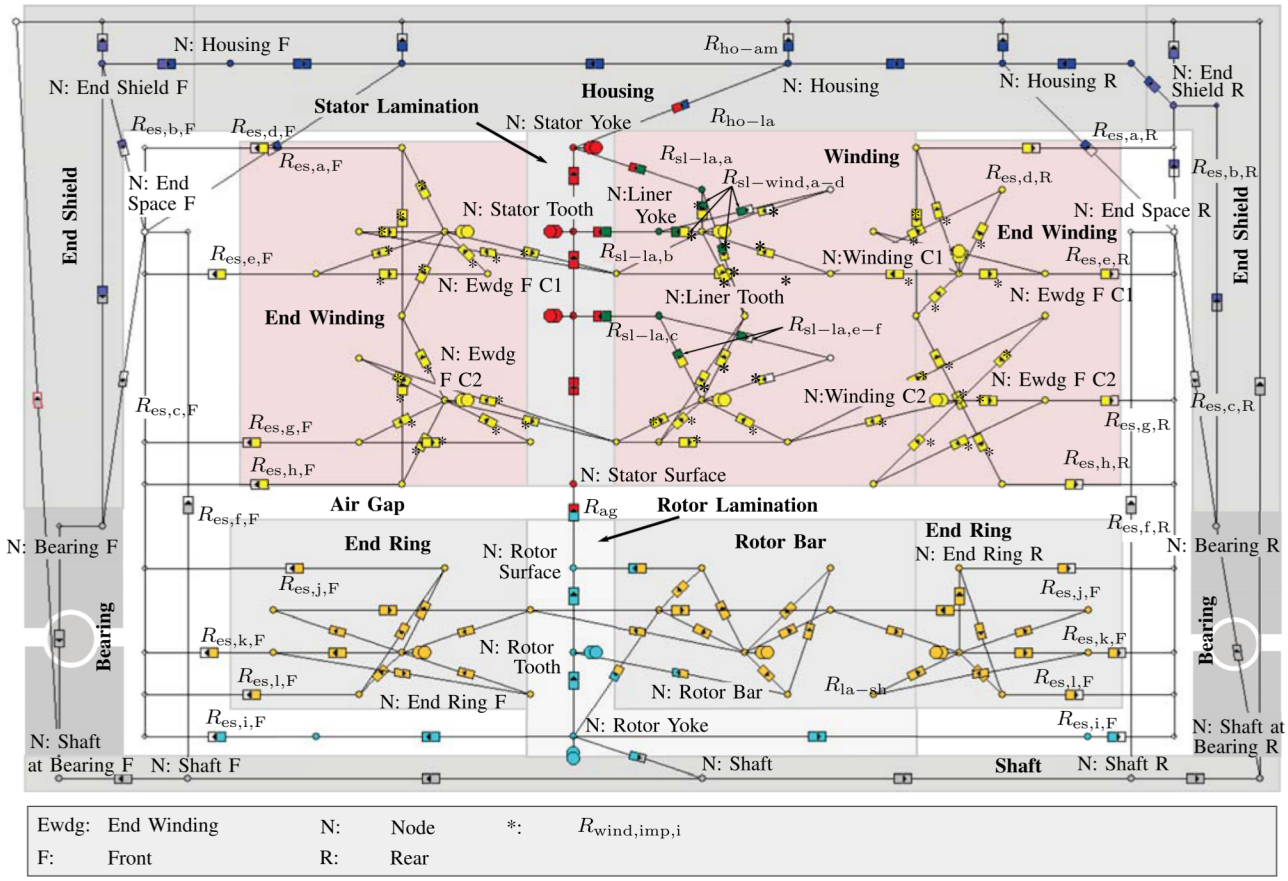

Fig. 2. LPTN of the studied IM.

with the rotational velocity of the inner cylinder ω, the average radius of the annulus r_{a}, the thickness of the annulus δ, and the kinematic viscosity of the air ν. The geometrical factor F_{G} is neglected, because its influence in electric machines with small δ is negligible. The most important alternative definition of Ta is the definition of Becker and Kay [15]. This definition is converted using the following formula:

$$Ta_{\mathrm{BK}} = \frac{\omega^2 r_{\mathrm{a}} \delta^3}{\nu^2} = Ta_{\mathrm{KE}}^2. \tag{2}$$

The general definition of the Nu-Number is given with

$$Nu = \frac{l_{\mathrm{th}} h}{k}, \tag{3}$$

with the heat transfer coefficient h and the thermal conductivity k. For this study, the characteristic length l_{th} of the thermal problem is defined as 2δ in accordance to [16]. It is important to note that different definitions of l_{th} can be found in literature. The authors in [14] use δ as the characteristic length l_{th} and thus describe the heat transfer from the annulus to either the stator or the rotor. All formulas using different definitions of Nu are converted to:

$$l_{\mathrm{th}} = 2\delta. \tag{4}$$

The resulting Nu-correlation in dependency of the Ta-Number is depicted in Fig. 3. Bjorklund *et al.* performed an

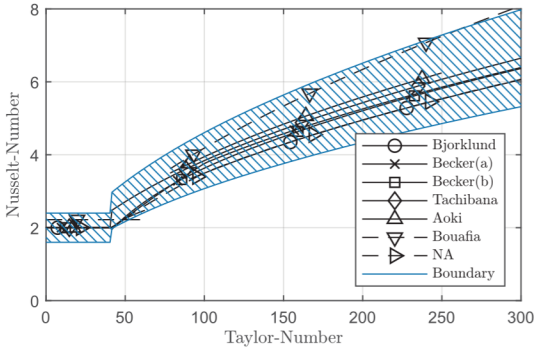

Fig. 3. Comparison of Nu-correlations for an annulus between two concentric cylinders with no axial flow.

experimental setup of a stationary hollow cylinder and a heated rotating inner cylinder with four different values of δ/r_{a} and air as a working fluid [17]. The investigation of Becker *et al.* used own measurement as well as data from two other studies. This study delivered a formulation with three different cases (a) and a formulation with two different cases (b), where the latter case includes both the transition area as well as the laminar flow regime with vortices [15]. In the report of Tachibana *et al.*, a study of three different fluids is described, i.e. oil, spindle oil and mobile oil [18]. Aioki *et al.* [19] performed measurements

with five different ratios of δ/r_{a} and four different fluids. He delivered different formula for the fluids, as it is challenging to fit all data for fluids with different Prandl-Numbers (Pr) into one formulation. The used formula in this study is recommended for air with Pr around 0.7. Bouafia *et al.* [20] performed measurements with a smooth airgap as well as a notched airgap. For the smooth case, the results coincident in a wide range of Ta with the other authors. For the notched case, they measured an increase in the heat transfer coefficient due to the changed flow pattern in the air gap. The sizes of the notches are significantly larger than those found in the two studied machines in this sensitivity study. Nevertheless, the authors demonstrate the interesting trend that the flow changes in a real annulus of an electric machine in comparison to the simplified smooth case. The last formula is added, because it is used as a state of the art formula in severeal publications in the field of thermal modeling of electric drives, such as [6], [21], [22]. Please note that the authors in [6] published a minor typo. The primary source of the literature could not be found after intensive literature research, but the correlation shows a comparable trend as depicted in Fig. 3. The results of Tachibana *et al.* are identified to be a well suited average value for this sensitivity study. For the upper and lower boundary, the resulting Nu-correlation is multiplied with a sensitivity factor for the annulus k_{an} that ranges from 0.8 to 1.2 in order to keep all curves within these boundaries. These boundaries are plotted in Fig. 3. The location of the corresponding thermal resistance in the air gap R_{ag} is labeled in the LPTN that is depicted in Fig 2.

C. Heat Transfer in the End Space

The heat transfer in the end space is a complicated heat transfer problem, where LPTN models have a significantly reduced accuracy. Models using Computational Fluid Dynamics (CFD) can lead to an increase of accuracy [5]. In this study, the influence of different analytical models found in literature are analyzed. A comprehensive description and discussion of the different definitions can be found in several literature such as [6], [21], [23]. A common formula of the authors [24]–[29] that introduced different definitions is:

$$h = k_{\mathrm{es},1}(1 + k_{\mathrm{es},2} v^{k_{\mathrm{es},3}}) \tag{5}$$

The first correlation factor $k_{\mathrm{es},1}$ describes the influence of natural convection. The two factors $k_{\mathrm{es},2}$ and $k_{\mathrm{es},3}$ describe the improvement of the thermal heat transfer coefficient by forced convection. The fluid velocity for the i-th component in the end space v_{i} is defined by the following equation:

$$v_{\mathrm{i}} = \omega_{\mathrm{rot}} r_{\mathrm{i}} k_{\mathrm{rot}} k_{\mathrm{i}} \tag{6}$$

with the rotational velocity of the rotor ω_{rot} and the radius of the surface of the component facing the end space r_{i}. The rotor surface factor k_{rot} defines the correlation between the rotor surface velocity and the reference velocity and depends on the roughness of the rotor surface. It is selected to be 0.5 representing a normal rotor without an added fan. The local velocity factors k_{i} represent the local velocities at each component i facing the end space. A comparison of the calculated heat transfer coefficients

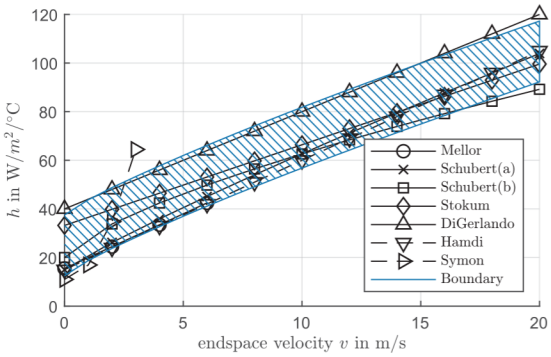

Fig. 4. Comparison of h-correlations for the end space.

in dependency of the fluid velocity is given in Fig. 4. In order to obtain a parameter that can be manipulated for the sensitivity study and that represents the variety of expressions shown in Fig. 4, an additional parameter $k_{\mathrm{es},4}$ is defined. This parameter is added to the formulation given in (5):

$$h = k_{\mathrm{es},1}(k_{\mathrm{es},4} + k_{\mathrm{es},2} v^{k_{\mathrm{es},3}}) \tag{7}$$

The highlighted boundary in Fig. 4 is defined with $k_{\mathrm{es},1} = 25\,\mathrm{W/(m^2\,K)}$, $k_{\mathrm{es},2} = 0.25$, and $k_{\mathrm{es},3} = 0.85$, where $k_{\mathrm{es},4}$ is varied between 0.5 and 1.5. The according resistances of the end space correlation in the LPTN in Fig. 2 are labeled with alphabetical indices $R_{\mathrm{es,a}}$ to $R_{\mathrm{es,l}}$.

D. Lamination to Housing Interface

The thermal resistance between two different materials can be modeled with a layer of air and thermal conduction. This equivalent interface gap thickness d_{ig} depends on several influencing parameters, such as the surface roughness, the contact pressure between the components, or the material hardness. [6] gives a comparison of interfaces found in general literature and self conducted measurements of the interface between housing and stator lamination. While general literature gives values of d_{ig} between $0.2\,\mu\mathrm{m}$ and $15.3\,\mu\mathrm{m}$, measurements in [6] indicate higher values between $10\,\mu\mathrm{m}$ and $77\,\mu\mathrm{m}$. The authors conclude that the complex interface in electric machines with laminated single sheets and the different thermal expansion coefficients are the reason for the increased values. The data given in [6] is expanded by the same research group [7] and the value range for d_{ig} between $10\,\mu\mathrm{m}$ and $77\,\mu\mathrm{m}$ is confirmed. Another measurement of the interface gap for motors with a power range between 80 W and 15 kW is given in [30]. The authors calculate an air layer thickness d_{ig} between $34\,\mu\mathrm{m}$ and $46\,\mu\mathrm{m}$ for four of the five machines with one outlier at $95\,\mu\mathrm{m}$. For this study, a variation of the d_{ig} between $10\,\mu\mathrm{m}$ and $77\,\mu\mathrm{m}$ is used. The corresponding resistance in the LPTN in Fig. 2 is labeled with $R_{\mathrm{ho-la}}$. Note that this resistance also includes the conductive share of the housing and the lamination material between the two nodes.

TABLE II
SLOT LINER MATERIAL AND MINIMUM THICKNESS d_{sl}

Material	k_{sl} in $\mathrm{W/(m\,K)}$	E_{bd} in $\mathrm{V/m}$	ϵ_{r}	d_{sl} in µm	$k_{\mathrm{sl}}/d_{\mathrm{sl}}$ in $\mathrm{W/(m^2\,K)}$
a	0.139	33	3.0	75	1853
b	0.230	20	4.0	98	2346
c	0.195	7.2	6.0	133	1466
d	0.141	40	3.1	77	1831

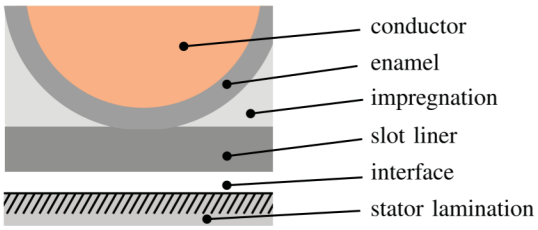

Fig. 5. Geometry of the electrostatic finite element simulation model.

E. Lamination to Shaft Interface

For the interface between the rotor lamination and the rotor shaft, the same boundary conditions as for the interface between the lamination and the housing are used with a range between $10\,\mu\mathrm{m}$ and $77\,\mu\mathrm{m}$. The corresponding resistance in Fig. 2 is labeled with $R_{\mathrm{la-sh}}$ and also includes the conductive share of the shaft and the lamination material between the two nodes.

F. Slot Liner and Lamination to Slot Liner Interface

Another interface region, which is modeled with an airgap with constant thickness, is placed between the slot liner and the stator lamination. Three different slot liners are studied in [31] and a tickness of d_{ig} between $50\,\mu\mathrm{m}$ and $60\,\mu\mathrm{m}$ is measured. For the sensitivity study, a range variation for this material interface of $30\,\mu\mathrm{m}$ and $80\,\mu\mathrm{m}$ is used. The lamination to slot liner interface is part of the resistance $R_{\mathrm{sl-la}}$ as depicted in Fig. 2. Another part of this resistance is the conductivity of the adjacent materials, i.e. the stator lamination and the slot liner. The latter influence parameter is studied in the next section.

G. Slot Liner

The slot liner material partially contributes to the previously introduced resistances $R_{\mathrm{sl-la,a-c}}$ as well as to $R_{\mathrm{sl-wind,a-f}}$ as depicted in Fig. 2. The resistance is calculated based on an equivalent thermal conductivity. Therefore, the performance of four different slot liner materials are studied.

a) Nomex 410 by Dupont
b) Therma Volt by 3 M
c) CeQUIN by 3 M
d) Nomex Kapton Nomex (NKN) by Dupont

The three materials a) – c) are introduced in [31]. They are qualified for a thermal class of 220 °C. Nomex is a trade name for polyaramid, a purely organic material. The other two insulation materials are based on polymeres, which are equipped with inorganic particles to increase their thermal conductivity. A fourth slot liner d) that is commonly used for the phase-to-ground insulation is the laminate NKN. This slot liner consists of a polyimide-layer (trade name Kapton), which is placed between two layers of Nomex. Thermal and electrical properties of the insulation materials are listed in Table II . The thermal resistance between the winding and the stator lamination depends on the thermal conductivity k_{sl} and the thickness of the insulation layer slotliner d_{sl}, which is calculated within this study. The minimum thickness however is limited by the minimum breakdown voltage, which is influenced by the dielectric strength E_{bd} and the relative permittivity ϵ_{r} of the material. The thermal conductivity k_{sl} and permittivity ϵ_{r} of material 4 (NKN) is calculated using a weighted average of Kapton and Nomex, with a Kapton layer thickness of 12.5% of the thickness of the slot liner.

For the evaluation of minimum necessary material thickness of each material, an electrostatic FE-Simulation model is set up with the geometry as depicted in Fig. 5. The effect of possible partial discharge as well es an electrical break-down in the slot liner material is investigated in the simulation. The properties for the enamel, the impregnation, and the interface gap are selected to represent the worst case for the two above mentioned effects, i.e. DC-voltage of 400 V, enameled wire grade 2, and a conductor diameter of 1 mm. According to [32], safety factors which take voltage overshoot, ageing, temperature and the bipolar voltages pulse voltage waveform of inverters into account are considered. A safety factor of 2.9 is used representing a machine with a short cable connection lower than 0.3 m. The thickness of the slot liner is reduced until either the minimum permissible breakdown- or the partial discharge inception voltage is reached. The minimum thickness of each material is added to Table II. The ratio of thermal conductivity k_{sl} and material thickness d_{sl} is calculated and the material with the highest value is selected, i.e. material b) with a $k_{\mathrm{sl}}/d_{\mathrm{sl}}$ of $2346\,\mathrm{W/(m^2\,K)}$. This value of $k_{\mathrm{sl}}/d_{\mathrm{sl}}$ represents the best case of the heat transition and the upper boundary for the simulation study. The lower boundary of the simulation study is determined using the material thickness of $0.35\,\mathrm{mm}$ as a typically used thickness in electric drives. Material a) is selected with the lowest thermal conductivity $k_{\mathrm{sl}} = 0.139\,\mathrm{W/(m\,K)}$, resulting in $k_{\mathrm{sl}}/d_{\mathrm{sl}} = 397\,\mathrm{W/(m^2\,K)}$.

H. Impregnation Material

The total thermal conductivity of the insulation material $k_{\mathrm{tot,imp}}$ is another studied influence parameter, which is calculated with

$$k_{\mathrm{tot,imp}} = x_{\mathrm{gn}} \cdot k_{\mathrm{imp}} + (1 - x_{\mathrm{gn}}) k_{\mathrm{air}}, \tag{8}$$

where x_{gn} is the goodness of impregnation and k_{imp} and k_{air} are the conductivity of the impregnation material and enclosed air respectively. The two parameters show an interdependence. Impregnation materials with high thermal conductivity tend to have an increased viscosity. This increased viscosity leads to

TABLE III
PROPERTIES OF WINDING IMPREGNATION MATERIAL

Material	Ref	k_{imp} in $\mathrm{W/(m\,K)}$	μ in $\mathrm{Pa\,s}$	x_{gn}	$k_{\mathrm{tot,imp}}$ in $\mathrm{W/(m\,K)}$
NA	[7]	0.13		0.3 - 0.5	0.06 - 0.08
Varnish	[33]	0.25		0.65 - 0.75	0.17 - 0.19
Epoxylite	[33]	0.85	3.5	0.65 - 0.75	0.56 - 0.14
sbTCM	[33]	3.20	25	0.55 - 0.65	1.77 - 2.41
study	min	0.25		0.65	0.17
study	max	2		0.6	1.21

challenges in the impregnation process, as the material might cure before the entire slot is filled. Due to this interdependence, the total thermal conductivity $k_{\mathrm{tot,imp}}$ is considered in this study and not both of the factors x_{gn} and k_{imp} individually. An overview of some results of a material impregnation study is given in Table III. In [7], four different industrial drives are investigated. All machines are manufactured with the same impregnation material with a thermal conductivity k_{imp} of $0.13\,\mathrm{W/(m\,K)}$. The examined goodness of impregnation x_{gn} varies between 0.3 and 0.5. The authors recommend to use higher values for highly utilized machines between 0.4 and 0.8, as the studied machines in [7] are industrial drives with low production cost. Three different impregnation materials are studied in [33]. The studied varnish is recommended for industrial or other low cost drives with low thermal requirements. As this study is focusing on high power density, this varnish is set as the lower boundary for the parameter study. The shown sbTCM material has a high thermal conductivity but a lower dielectric strength of about 50% of Epoxylite. Another disadvantage of the sbTCM material is the high price and the high viscosity of the material [33]. The authors [33] built up a prototype with an axial length of $105\,\mathrm{mm}$ without issues. In this study, the axial length of both machines with $200\,\mathrm{mm}$ and $131\,\mathrm{mm}$ for the IM and the PMSM respectively and the achievable thermal conductivity k_{imp} of $3.2\,\mathrm{W/(m\,K)}$ seems to be too high. The maximum value of this study is assumed to be lower with a thermal conductivity k_{imp} of $2\,\mathrm{W/(m\,K)}$. The resulting minimum and maximum values for the total impregnation thermal conductivity k_{totimp} are calculated for the different values using (8) and are depicted in Table III. Reference or literature source (Ref) is added to the overview. The winding of the machine is represented by cuboidal elements as introduced in [13]. The thermal conductivity k_{totimp} is used for the calculation of the resistances of the elements $R_{\mathrm{wind,imp,i}}$ as described in [13]. The influence of the impregnation is so considered in the resistances, labeled with $R_{\mathrm{wind,imp,i}}$ in the LPTN in Fig. 2.

IV. SENSITIVITY STUDY

A. Operational Points

Two different operational points for each machine are selected. The first operational point OP1 is at the rated speed as shown in Table I, the second operational point OP2 is selected at the double value of the rated speed representing operation at high speed and in the field weakening range. The torque of the machines is increased until the maximum permitted component temperatures are reached, i.e. $120\,^{\circ}\mathrm{C}$ for the permanent magnets, $180\,^{\circ}\mathrm{C}$ for the winding, and $250\,^{\circ}\mathrm{C}$ for the rotor bars. The torque of the PMSM is set to $210\,\mathrm{Nm}$ for OP1 and to $80\,\mathrm{Nm}$ for OP2. The torque of the studied IM is set to $64\,\mathrm{Nm}$ for OP1 and to 34 Nm for OP2.

TABLE IV
OVERVIEW OF THE FACTORS OF THE DOE

	Description	Variable	LB	UB
A	primary cooling factor	k_{pc}	0.8	1.2
B	rotor stator annulus factor	k_{an}	0.8	1.2
C	end space factor	$k_{\mathrm{es},4}$	0.8	1.2
D	gap lamination housing	$d_{\mathrm{ig,la,ho}}$ in µm	10	77
E	gap lamination shaft	$d_{\mathrm{ig,la,sh}}$ in µm	10	77
F	gap slot liner lamination	$d_{\mathrm{ig,la,sl}}$ in µm	30	80
G	slot liner	$k_{\mathrm{sl}}/d_{\mathrm{sl}}$ in $\mathrm{W/(m^2\,K)}$	397	2346
H	impregnation material	$k_{\mathrm{tot,imp}}$ in $\mathrm{W/(m\,K)}$	0.17	1.21

B. Methodology and Boundary Conditions

A fully factorial simulation plan is selected for the Design of Experiments (DOE) approach. The upper boundary (UB) and lower boundary (LB) of the eight factors (A to H) are selected based on the previously discussed findings and are depicted in Table IV. The number of factors is eight, resulting in a total of 256 thermal steady state simulations for each machine and operational point. The maximum temperature of the winding $T_{\mathrm{max,wind}}$ is the first evaluated effect for both machines. The second evaluated effect is the magnet temperature $T_{\mathrm{max,mag}}$ for the PMSM and the rotor bar temperature $T_{\mathrm{max,rb}}$ for the IM. The shown factors are used for both the parameterization process and the sensitivity study.

V. DEFINITION OF MEASUREMENT SYSTEM AND EXPERIMENTAL VALIDATION

In order to obtain suitable accuracy for the sensitivity study, both machines are measured on a test bench.

A. Validation of the Studied PMSM

A detailed description of the setup and the parameterization process of the studied PMSM is given in [3]. The end-winding temperatures of 12 different operational points are used to parameterize the LPTN model. A maximum deviation of measurement and simulation of 5 K for all operational points is achieved for the PMSM [3]. The heat transfer coefficient for the primary cooling of the housing cooling channels is defined by an analytical approach as described in [3] with $1400\,\mathrm{W/(m^2\,K)}$. This coefficient is multiplied by the correlation factor A in the later sensitivity study. Factor B with k_{an} has a value of 0.84. The resulting end space correlation uses $k_{\mathrm{es},1} = 15\,\mathrm{W/(m^2\,K)}$, $k_{\mathrm{es},2} = 0.4$, and $k_{\mathrm{es},3} = 0.9$. It cannot be directly compared to the used Factor C, but the resulting heat transfer coefficients are

TABLE V
DIFFERENCES BETWEEN TEMPERATURES OF SIMULATION T_s AND MEASUREMENT T_m OF THE STUDIED IM

	OPM		Winding			Rotor Bar		
	T in N m	n in rpm	T_m °C	T_s °C	δ %	T_m °C	T_m °C	δ %
1	100	100	126	130	+3.1	83	82	-0.8
2	60	1900	112	113	+1.1	137	139	+1.4
3	60	3700	135	130	-3.8	172	177	+2.9
4	38	5700	135	130	-3.6	175	176	+0.8
5	26	7500	134	124	-8,0	172	166	-3.2

all within the boundaries as defined by Factor C and depicted in Fig. 4. The gap between lamination and housing $d_{\mathrm{ig,la,ho}}$ is identified to be $21\,\mu\mathrm{m}$ (Factor D). The interface between rotor lamination and shaft $d_{\mathrm{ig,la,sh}}$ (Factor E) is at the lower boundary of the studied range. As shown later in the result section, this parameter has almost no influence on the studied temperatures. The given values can thus not be seen as validated and should not be seen as granted. The gap of the slot liner to lamination with Factor F ($d_{\mathrm{ig,la,sl}}$) is close the lower boundary with $35\,\mu\mathrm{m}$. The value of Factor G $k_{\mathrm{sl}}/d_{\mathrm{sl}}$ has a value of $519\,\mathrm{W/(m\,K^2)}$. The values for the impregnation material $k_{\mathrm{tot,imp}}$ with Factor H is $0.25\,\mathrm{W/(m\,K)}$.

B. Validation of the Studied IM

For the parameterization of the IM, a test bench setup and measurements as introduced in [34] are used. The development of a low order LPTN based on this measurement data is given in [2]. In this study, a more complex LPTN, as depicted in Fig. 2, is developed and parameterized using this measurement data. In addition to the four operational points as described in [2], one additional point is evaluated at very low speed, i.e. OPM1 at 100 Nm and 100 rpm. The load can only be applied for a short term operation S2 (5 min) for OPM1. The other operational points are run for a short term operation S2 of 30 min. The winding temperatures and the rotor bar temperature are measured. An overview of the five operational points of the measurement (OPM) including a comparison of the simulated and measured temperatures is given in Table V.

The results show good agreement within a deviation of 4% with one outlier of the winding temperature for OPM5 with 8%. A comparison of the temperature curves for one OPM with 5 min operation (OPM1) and one OPM with 30 min operation (OPM2) is given in Fig. 6. It is interesting to note some difference in evaluation between the data presented in Table V and Fig. 6. While temperature curves in Fig. 6 coincident very well with measurement data for OPM1, a difference of 3.1% is recorded in the data of the maximum temperature in Table V. The limited response behavior of the measurement systems leads to a flattening of the temperature at the vertex of the curve, i.e. where the operational mode is changed from heating to cooling. The effect occurs at highly transient operation such as found in OPM1 and leads to a lower evaluated temperature in the data comparison of Table V.

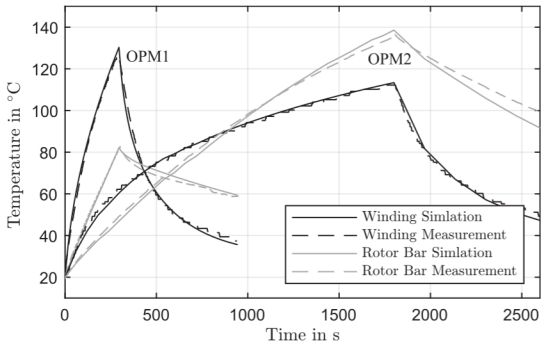

Fig. 6. Comparison of measured and simulated temperatures of the studied IM for OPM1 and OPM2.

In the following, the identified parameters are discussed for the studied IM. Factor A represents the heat transfer coefficient of the primary cooling. The heat transfer coefficient h is varied in a range of $20\,\mathrm{W/(m^2\,K)}$ and $300\,\mathrm{W/(m^2\,K)}$ and is identified to be $80\,\mathrm{W/(m^2\,K)}$. Note that this value is slightly lower than the identified value in the reduced lumped parameter model which is published in [3]. Factor B with k_{an} is identified to be 1.2. The resulting end space correlation cannot directly be compared to $k_{\mathrm{es},4}$, because the Schubert (a) correlation as depicted in Fig. 4 is identified to be the best suited end space correlation with $k_{\mathrm{es},1} = 15\,\mathrm{W/(m^2\,K)}$, $k_{\mathrm{es},2} = 0.4$, and $k_{\mathrm{es},3} = 0.9$. As depicted in Fig. 4, this correlation is well within the studied range of the sensitivity study. The gap between lamination and housing $d_{\mathrm{ig,la,ho}}$ is identified to be $14\,\mu\mathrm{m}$. Note that the equivalent value for the resistance between the housing and the stator lamination of the low order LPTN as published in [3] is higher, because the conductivity of the lamination and the housing is included in [3], but excluded in this study. The interface between rotor lamination and shaft $d_{\mathrm{ig,la,sh}}$ is at the lower boundary of the studied range. As shown later in the result section, this parameter has almost no influence on the studied temperatures. The given value can thus not be seen as validated and should not be seen as granted. The gap of the slot liner to lamination with Factor F ($d_{\mathrm{ig,la,sl}}$) is identified to be $55\,\mu\mathrm{m}$. Factor F shows significant influence on the temperature curves in OP1 during parameterization, because the temperatures of the winding and the stator lamination adjust rapidly for low interface gaps and thus influence highly dynamical operational points. The value of Factor G $k_{\mathrm{sl}}/d_{\mathrm{sl}}$ is at the lower level for the studied IM with a value of $400\,\mathrm{W/(m^2\,K)}$. The values for the impregnation material with Factor H is identified to be $0.25\,\mathrm{W/(m\,K)}$ for the IM. Please be aware that some of the parameterized values show strong interdependencies. As an example, the influence of the gap between slot liner and stator lamination and the thermal conductivity of the slot liner cannot be separated completely.

VI. RESULTS AND DISCUSSION

The influence results of the sensitivity study are shown in Fig. 7. The eight factors on the two effects of each machine per operational point are analyzed. The main effect of each factor using the average values is depicted as a black line that connects

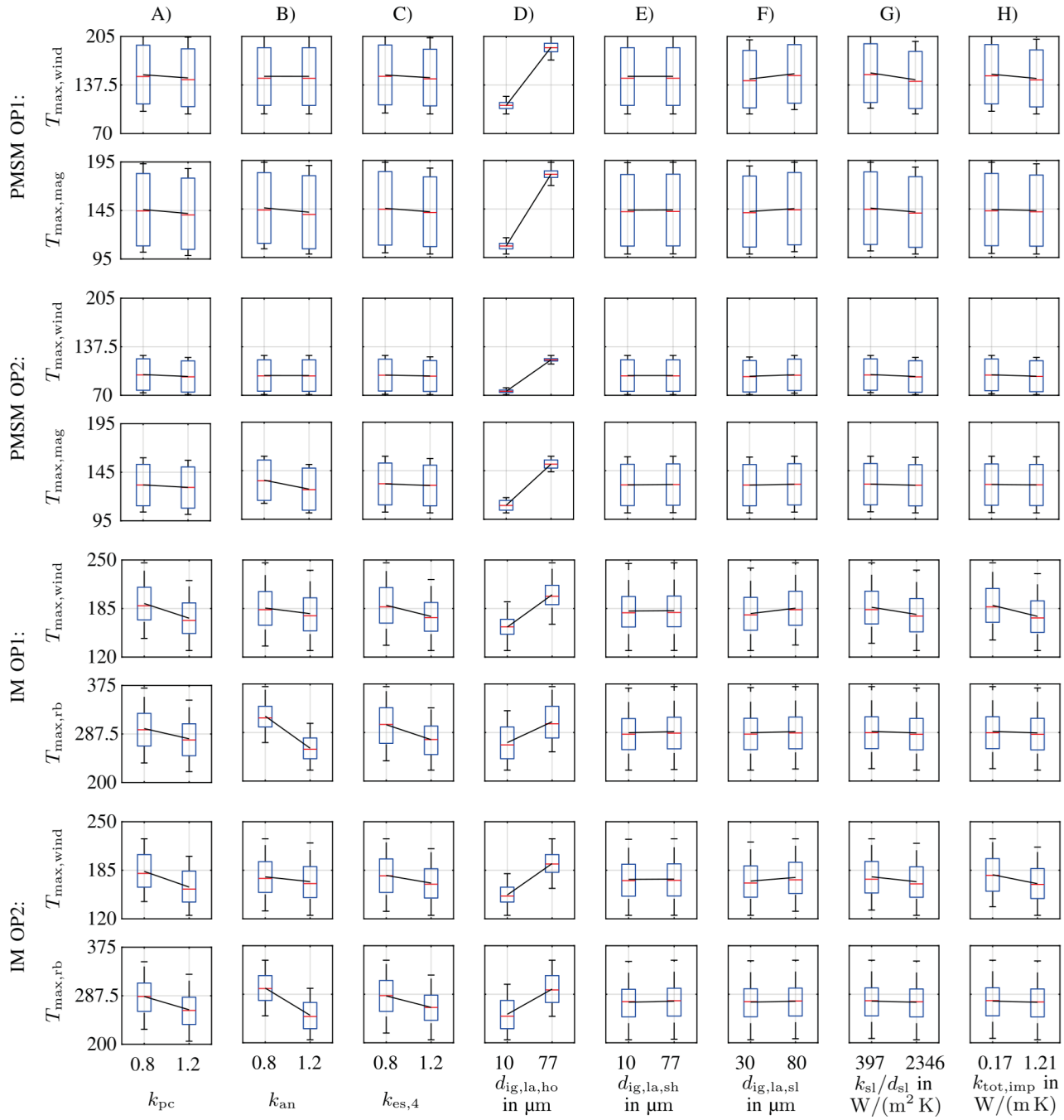

Fig. 7. Influence of the eight factors on the two effects per studied machine and operational point in °C.

the two boxes. The median of the resulting effects for the lower or upper boundary is plotted as a red horizontal line placed inside of each box. The 25- and 75-percentiles of the deviation are represented by the blue box. The minimum and maximum values are depicted by the bar above and below the blue box.

The winding temperature of the studied PMSM shows higher average values in the base speed region (OP1) than in the field weakening region (OP2). The magnet temperatures of the PMSM show a more similar behavior for the two operational points. The difference is driven by the frequency influence of the iron losses. An increase of rotational velocity leads to an increase of the share of rotor iron losses on the overall losses. Factor A, which represents the deviation of the heat transfer coefficient of the primary cooling k_{pc}, shows a minor influence for the studied PMSM. The influence for the IM is more significant. The housing water jacket cooling of the PMSM with $h = 1400\,\mathrm{W/(m^2\,K)}$ is significantly more efficient than the forced air cooling of the studied IM with $h = 80\,\mathrm{W/(m^2\,K)}$. The thermal resistance of the convective heat transfer in the LPTN of the IM is a more critical bottle neck to the overall design. Thus, the influence of a change in this resistance on

the temperature is more significant for the IM. The influence of Factor A is similar for both operational points for each machine. This similar behavior is reasonable as the studied resistance represents the last resistance in the heat path before arriving the sink. A similar amount of extracted heat leads to a similar temperature drop in the resistance. The heat transfer between the stator and rotor annulus, which is represented by factor B with k_{an}, is the most influential factor for the rotor bar temperature $T_{\mathrm{max,rb}}$ of the studied IM. This result is obvious, as the main portion of the rotor losses are extracted by the heat path of the annulus of the machine in case of solely stator cooling. The influence of Factor B depends on the studied operational point. For the PMSM, the influence is more significant for high speed operation in OP2. The effect occurs due to the higher share of rotor losses caused by increased iron losses in the rotor. It is interesting to note that the resistance in the annulus shows a clear influence on the stator winding temperature for the studied IM. This influence is independent on the rotational speed and is caused by the cross coupling of different heat paths within the machine. The generated heat in the rotor is constant at a studied operational point and needs to be extracted in thermal steady state. In case the heat extraction of the rotor losses over the annulus is simplified, less heat has to be extracted by the heat path over the end space, where the end winding is adjacent. The influence of the end space correlation, which is represented by factor C, plays a minor role for the PMSM. Due to the higher rotor losses of the IM, the influence of the factor is more significant for the IM than for the PMSM. The most influential factor on all effects of the studied PMSM is factor D that represents the gap between the housing and the stator lamination $d_{\mathrm{ig,la,ho}}$. Factor D not only influences the maximum winding temperature $T_{\mathrm{max,wind}}$, but also shows significant impact on the maximum magnet temperature $T_{\mathrm{max,mag}}$. This influence is caused by the heat flow from the rotor over the stator into the housing for a machine with solely housing cooling. An increase in the thermal resistance leads to increased temperature drop over the interface for the heat extraction paths of the rotor and the stator. Factor E shows a minor impact on the studied effects, because no significant heat path is conducted over the rotor lamination to the shaft interface. The three factors F, G, and H represent the characteristic parameters of the winding system, i.e. the gap between the slot liner and the lamination, the slot liner, and the impregnation material respectively. At first sight, the impact on the effects correlated to the maximum winding temperature $T_{\mathrm{max,wind}}$ seems to be minor. A detailed analysis of the main effects shows a more significant influence. As an example, the influence of factor F on the $T_{\mathrm{max,wind}}$ of the IM for OP1 can be analyzed. The main effect of factor F is 7.1 K, of factor G is 9.6 K, and of factor H is 14.7 K. The total potential of the three factors is 31.4 K. Especially the potential of factor G representing the slot liner needs to be considered in future applications. Please also note that both machines are designed for DC-voltages below 400 V. The usage of higher-voltage DC links leads to necessity of increased insulation requirements for the wire enamel and slot liner. Meeting these requirements normally leads to drawbacks on the thermal extraction of the generated winding losses of the machine.

VII. Conclusion

Electromagnetic and thermal simulation models for two different drives are developed and parameterized by using test bench measurements for the model calibration. The resulting curves of temperature rise show good agreement with the measurements. The performed sensitivity analysis is used to identify the critical thermal parameters of each studied motor and operational point. As all identified parameters during the test bench evaluation are within the boundaries of the sensitivity analysis, the approach can also be used in an early design stage without test bench evaluation. It can be used to identify trends and crucial thermal design parameters. The study illustrates that more advanced models such as CFD not always lead to an improved significance of the overall model. The interface modeling such as found in the stator lamination to housing interface plays a significant role in the thermal modeling of the studied electric drives. The study shows that the influence of the thermal parameters on maximum component temperatures varies in dependency of the used machine topology, the used cooling technology as well as the studied operational point. The methodology can be used in an early design stage to identify the critical parameters for a specific design under defined operational conditions.

References

[1] M. Popescu, D. A. Staton, A. Boglietti, A. Cavagnino, D. Hawkins, and J. Goss, "Modern heat extraction systems for power traction machines–A review," *IEEE Trans. Ind. Appl.*, vol. 52, no. 3, pp. 2167–2175, May/Jun. 2016.

[2] B. Groschup, S. Elfgen, and K. Hameyer, "Iron loss simulation using a local material model," *COMPEL - Int. J. Comput. Math. Elect. Electron. Eng.*, vol. 38, no. 4, pp. 1224–1234, 2019.

[3] B. Groschup, M. Komissarov, S. Stevic, and K. Hameyer, "Operation enhancement of permanent magnet excited motors with advanced rotor cooling system," in *Proc. IEEE Transp. Electrific. Conf. Expo.*, 2019, pp. 1–6.

[4] S. Y. Goh, J. Wale, and D. Greenwood, "Thermal analysis for stator slot of permanent magnet machine," in *Proc. 22nd Int. Conf. Elect. Mach.*, 2016, pp. 2093–2098.

[5] A. Boglietti, S. Nategh, E. Carpaneto, L. Boscaglia, and C. Scema, "An optimization method for cooling system design of traction motors," in *Proc. IEEE Int. Electric Mach. Drives Conf.*, 2019, pp. 1210–1215.

[6] D. Staton, A. Boglietti, and A. Cavagnino, "Solving the more difficult aspects of electric motor thermal analysis in small and medium size industrial induction motors," *IEEE Trans. Energy Conver.*, vol. 20, no. 3, pp. 620–628, Sep. 2005.

[7] A. Boglietti, A. Cavagnino, and D. A. Staton, "Determination of critical parameters in electrical machine thermal models," *IEEE Trans. Ind. Appl.*, vol. 44, no. 4, pp. 1150–1159, Jul./Aug. 2008.

[8] F. Zhang, D. Gerada, Z. Xu, H. Zhang, and C. Gerada, "Sensitivity analysis of machine components thermal properties effects on winding temperature," in *Proc. 22nd Int. Conf. Electric Mach. Syst.*, 2019, pp. 1–5.

[9] B. Assaad, K. El kadri Benkara, S. Vivier, G. Friedrich, and A. Michon, "Thermal design optimization of electric machines using a global sensitivity analysis," *IEEE Trans. Ind. Appl.*, vol. 53, no. 6, pp. 5365–5372, Nov./Dec. 2017.

[10] A. Boglietti, A. Cavagnino, and D. A. Staton, "Tefc induction motors thermal models: A parameter sensitivity analysis," *IEEE Trans. Ind. Appl.*, vol. 41, no. 3, pp. 756–763, May/Jun. 2005.

[11] N. Leuning, S. Elfgen, B. Groschup, G. Bavendiek, S. Steentjes, and K. Hameyer, "Advanced soft- and hard-magnetic material models for the numerical simulation of electrical machines," *IEEE Trans. Magn.*, vol. 54, no. 11, pp. 1–8, Nov. 2018.

[12] G. von Pfingsten, S. Steentjes, and K. Hameyer, "Operating point resolved loss calculation approach in saturated induction machines," *IEEE Trans. Ind. Electron.*, vol. 64, no. 3, pp. 2538–2546, Mar. 2017.

[13] R. Wrobel and P. H. Mellor, "A general cuboidal element for three-dimensional thermal modelling," *IEEE Trans. Magn.*, vol. 46, no. 8, pp. 3197–3200, Aug. 2010.
[14] J. Kaye and E. C. Elgar, "Modes of adiabatic and diabatic fluid flow in an annulus with an inner rotating cylinder," *Trans. ASME*, vol. 80, pp. 753–765, 1958.
[15] K. M. Becker and J. Kaye, "Measurements of diabatic flow in an annulus with an inner rotating cylinder," *J. Heat Transfer*, vol. 84, no. 2, pp. 97–104, 1962.
[16] C. Gazley, Jr, "Heat-transfer characteristics of the rotational and axial flow between concentric cylinders," *Trans. ASME*, vol. 80, pp. 79–90, 1958.
[17] I. S. Bjorklund and W. M. Kays, "Heat transfer between concentric rotating cylinders," *J. Heat Transfer*, vol. 81, no. 3, pp. 175–183, 1959.
[18] F. Tachibana, S. Fukui, and H. Mitsumura, "Heat transfer in an annulus with an inner rotating cylinder," *Trans. Jpn. Soc. Mech. Engineers*, vol. 25, no. 156, pp. 788–792, 1959.
[19] H. Aoki, H. Nohira, and H. Arai, "Convective heat transfer in an annulus with an inner rotating cylinder," *Bull. JSME*, vol. 10, no. 39, pp. 523–532, 1967.
[20] M. Bouafia, Y. Bertin, J. Saulnier, and P. Ropert, "Experimental analysis of the heat transfer in a narrow and grooved annulus with rotating inner cylinder," *Int. J. Heat Mass Transfer*, vol. 41, no. 10, pp. 1279–1291, 1998.
[21] D. A. Staton and A. Cavagnino, "Convection heat transfer and flow calculations suitable for analytical modelling of electric machines," in *Proc. IECON 32nd Annu. Conf. IEEE Ind. Electron.*, 2006, pp. 4841–4846.
[22] M. Bouchaala, H. Surin, and J. C. Vannier, "Thermal analysis of a small dc motor," in *Proc. Int. Intell. Motion Conf.*, 1995, pp. 275–286.
[23] G. L. Basso, J. Goss, Y. C. Chong, and D. Staton, "Improved thermal model for predicting end-windings heat transfer," in *IEEE Energy Convers. Congr. Expo.*, 2017, pp. 4650–4657.
[24] P. H. Mellor, D. Roberts, and D. R. Turner, "Lumped parameter thermal model for electrical machines of tefc design," *IEEE Proc. B. - Electric Power Appl.*, vol. 138, no. 5, pp. 205–218, Sep. 1991.
[25] E. Schubert, "Heat transfer coefficients at end winding and bearing covers of enclosed asynchronous machines," *Elektrie*, vol. 22, no. 1, pp. 160–162, 1968.
[26] H. D. Symons and M. Walker, "The heat paths in electrical machinery," *J. Inst. Elect. Engineers*, vol. 48, no. 213, pp. 674–718, 1912.
[27] A. D. Gerlando and I. Vistoli, "Improved thermal modelling of induction motors for design purposes," *Proc. 6th Int. Conf. Elect. Mach. Drives*, 1993, pp. 381–386.
[28] E. S. Hamdi, *Design of Small Electrical Machines*. Chichester, U.K.: John Wiley & Sons, Inc., 1994.
[29] G. Stokum, "Use of the results of the four-heat run method of induction motors for determining thermal resistance," *Elektrotechnika*, vol. 62, no. 6, pp. 219–232, 1969.
[30] W. Wang, Y. Zhou, and Y. Chen, "Investigation of lumped-parameter thermal model and thermal parameters test for ipmsm," in *Proc. 17th Int. Conf. Elect. Mach. Syst.*, 2014, pp. 3246–3252.
[31] R. Wrobel, S. J. Williamson, J. D. Booker, and P. H. Mellor, "Characterizing the in situ thermal behavior of selected electrical machine insulation and impregnation materials," *IEEE Trans. Ind. Appl.*, vol. 52, no. 6, pp. 4678–4687, Nov./Dec. 2016.
[32] *Rotating electrical machines - Part 18-41: Partial discharge free electrical insulation systems (Type I) used in rotating electrical machines fed from voltage converters - Qualification and quality control tests*, IEC 60034-18-41:2014, Mar. 2014.
[33] S. Nategh, A. Krings, O. Wallmark, and M. Leksell, "Evaluation of impregnation materials for thermal management of liquid-cooled electric machines," *IEEE Trans. Ind. Electron.*, vol. 61, no. 11, pp. 5956–5965, Nov. 2014.
[34] M. M. Nell, G. von Pfingsten, and K. Hameyer, "Rapid parameter identification and control of an induction machine," *Int. J. Comput. Math. Elect. Electron. Eng.*, vol. 37, no. 5, pp. 1678–1688, 2018.

Benedikt Groschup recieved the master's degree in automotive engineering and transport from RWTH Aachen University, Aachen, Germany, in 2015, in colaboration with Ford Motor Company in Detroit, MI, USA. In February 2016, he started working as a Research Associate with RWTH Aachen University. His research interests include induction and permanent magnet motor modeling, iron loss calculation in macroscopic scale, vehicle modeling, and thermal modeling.

Martin Nell received the master's degree in electrical engineering from RWTH Aachen University, Aachen Germany, in 2017. Since May 2017, he has been working as a Research Associate with the Institute of Electrical Machines. His research interests include induction machine modeling, optimization of induction machines, iron loss calculation in macroscopic scale, and vehicle modeling.

Florian Pauli received the master's degree in electrical engineering from RWTH Aachen University, Aachen, Germany, in 2017. Since May 2017, he has been working as a Research Associate with the Institute of Electrical Machines. His research interests include iron loss computations, thermal behavior, overload capability, lifetime models, and the characterization of insulation systems of electrical machines.

Kay Hameyer (Senior Member, IEEE) received the M.Sc. degree in electrical engineering from Leibniz University Hannover and the Ph.D. degree from the Technical University of Berlin, Berlin, Germany. He was with the Robert Bosch GmbH, Stuttgart, Germany, as a Design Engineer for permanent magnet servo motors and vehicle board net components. From 1996 to 2004, he was a full Professor for Numerical Field Computations and Electrical Machines with the Katholieke Universiteit Leuven, Leuven, Belgium. Since 2004, he has been a Full Professor and the Director of the Institute of Electrical Machines, RWTH Aachen University, Aachen, Germany. In 2006, he was Vice Dean of the faculty and from 2007 to 2009, he was the Dean of the faculty of Electrical Engineering and Information Technology, RWTH Aachen University. He has authored or coauthored more than 250 journal publications, more than 700 international conference publications, and authored four books. His research interests include numerical field computation and optimization, the design and controls of electrical machines, in particular permanent magnet excited machines, and induction machines. Since several years, his work is concerned with magnetically excited audible noise in electrical machines, the life time estimation of insulating systems and the characterization of ferromagnetic materials. He is a Member of VDE and fellow of the IET.